Solar signal propagation: the role of gravity waves and stratospheric sudden warmings

I. Cnossen[1], H. Lu[1], C.J. Bell[2], L.J. Gray[2] and M.M. Joshi[2]

[1]British Antarctic Survey, High Cross, Madingley Road, Cambridge CB3 0ET, United Kingdom

[2]University of Reading, Department of Meteorology, Reading RG6 6BB, United Kingdom

Abstract

We use a troposphere-stratosphere model of intermediate complexity to study the atmospheric response to an idealized solar forcing in the subtropical upper stratosphere during Northern Hemisphere (NH) early winter. We investigate two conditions that could influence the poleward and downward propagation of the response: 1) the representation of gravity wave effects, and 2) the presence/absence of Stratospheric Sudden Warmings (SSWs). We also investigate how the perturbation influences the timing and frequency of SSWs. Differences in the poleward and downward propagation of the response within the stratosphere are found depending on whether Rayleigh friction (RF) or a gravity wave scheme (GWS) is used to represent gravity wave effects. These are likely related to differences in planetary wave activity in the GWS and RF versions, as planetary wave redistribution plays an important role in the downward and poleward propagation of stratospheric signals. There is also remarkable sensitivity in the tropospheric response to the representation of the gravity wave effects. It is most realistic for GWS. Further, tropospheric responses are systematically different dependent on the absence/presence of SSWs. When only years with SSWs are examined, the tropospheric signal appears to have descended from the stratosphere, while the signal in the troposphere appears disconnected from the stratosphere when years with SSWs are excluded. Different troposphere-stratosphere coupling mechanisms therefore appear to be dominant for years with and without SSWs. The forcing does not affect the timing of

SSWs, but does result in a higher occurrence frequency throughout NH winter. Quasi-Biennial Oscillation effects were not included.

1. Introduction

Variations in solar ultraviolet (UV) irradiance that take place over the 11-year solar cycle are known to affect the upper stratosphere, where UV absorption by ozone takes place [Hood et al., 1993; Haigh, 1994, 1996; Gray et al., 2010]. Increased UV irradiance at solar maximum produces not only extra absorption directly, but also enhances the ozone concentration, making the equatorial upper stratosphere 1.5-2.5 K warmer compared to solar minimum [Hood, 2004; Crooks and Gray, 2005; Frame and Gray, 2010]. An even larger temperature signal associated with the 11-year solar cycle has been observed in the high latitude regions of the lower stratosphere, which is particularly strong during winter [Labitzke and Van Loon, 1988; Gray et al., 2004; Lu et al., 2009]. However, direct effects of changes in solar irradiance appear to be too small to cause these high latitude signals [Hood, 2004; Gray et al., 2009]. It has therefore been proposed that the solar UV forcing originating in the upper equatorial stratosphere may propagate dynamically poleward and downward during winter [Kodera and Kuroda, 2002; Matthes et al., 2004, 2006].

Kodera and Kuroda [2002] proposed a propagation mechanism involving the redistribution of planetary wave forcing during Northern Hemisphere (NH) winter. They suggested that a region of anomalously strong westerlies in the subtropical upper stratosphere/lower mesosphere during solar maximum, in thermal wind balance with an enhanced pole-to-equator temperature gradient in the upper stratosphere due to enhanced equatorial heating, may deflect planetary waves poleward. The redistribution of planetary wave forcing towards higher latitudes further strengthens the polar vortex in the subtropics, so that the zonal wind there becomes even more westerly. As the area of

anomalous westerly winds expands, this causes a further deflection of planetary waves, and so on, so that the westerly anomaly gradually moves poleward and downward.

This mechanism was demonstrated in a simple idealized modelling study by Gray et al. [2004], who imposed a small easterly anomaly in the subtropical upper stratosphere in early winter, representative of solar minimum. This resulted in a consistently more disturbed winter with a weaker vortex and earlier sudden warming events compared to their unforced integrations. Matthes et al. [2004, 2006] successfully reproduced this same behaviour in the NH winter using a more realistic full general circulation model, the Freie Universität Berlin Climate Middle Atmosphere Model (FUB-CMAM), and obtained a pattern of poleward and downward propagation of zonal wind anomalies, similar to observations. However, their modelled signal was much weaker than the observed signals. Also other studies with full chemistry-climate models and realistic solar forcing typically find signals that are weaker than seen in observations or at least at the lower end of observed ranges of peak responses [e.g. Marsh et al., 2007; Austin et al., 2008]. Matthes et al. [2004] argued that this could be due to the low variability produced by their model, as the amplitude of the response to solar forcing may be related to the amplitude of inter-annual variability [see also Kodera et al., 2003]. Kodera et al. [2003] further noted that the lower mesosphere subtropical jet was not very well reproduced in these simulations, which they suggested may be due to the use of Rayleigh friction as a crude parameterization of gravity wave forcings in the FUB-CMAM.

Rayleigh friction has long been the traditional approach to account for gravity wave effects, but is a rather crude method. It simply assumes that a drag must be present that is proportional to the ambient wind speed, with a height-dependent proportionality factor that is tuned such that a realistic climatology is obtained. It has several drawbacks. Firstly, it is usually applied uniformly in time, latitude and longitude, while real gravity wave sources and breaking events are likely to vary with location and be intermittent [Fritts and Alexander, 2003]. Secondly, it assumes that wave breaking always results in a drag on the mean wind, while in reality it may also accelerate winds in

some cases, depending on the wave characteristics and background wind itself. Thirdly, Rayleigh friction does also not conserve momentum [Shepherd et al., 1996; Shepherd and Shaw, 2004].

A more sophisticated way to account for gravity wave effects that relieves some of these problems is by means of a gravity wave parameterization that incorporates some representation of the wave breaking process. This then determines where and when the waves break, and whether they strengthen or weaken the winds as they do so, depending on the wave characteristics and background winds. The first of such parameterizations were already formulated by Lindzen [1981] and Dunkerton [1982], and since then have proven their value in many modelling studies [Fritts and Alexander, 2003]. It has been shown recently that the use of a gravity wave parameterization, as opposed to Rayleigh friction, can influence the modelled atmospheric response to a CO_2 forcing [Sigmond et al., 2008; Cnossen et al., 2009; Sigmond and Scinocca, 2010].

There is some evidence that this may be the case for solar forcings as well. Shibata and Kodera [2005] compared the results obtained with a traditional Rayleigh friction approach in their model to those obtained with the parameterization described by Hines [1997]. They found that the Hines parameterization produced a more realistic semi-annual oscillation (SAO). Differences in the response to solar forcing between the Rayleigh friction and gravity wave scheme versions of their model were therefore interpreted as being due to the absence/presence of the SAO. Further, McCormack et al. [2007] showed that a reduction in Rayleigh friction strength resulted in a more robust solar cycle modulation of the quasi-biennial oscillation (QBO), due to a larger solar cycle variation in model dynamics near the stratopause. These studies thus indicate that the representation of gravity wave effects can have consequences for the atmospheric response to solar forcing.

The first objective of this study is to investigate such influences in more detail. We do this in an extension of the study of Gray et al. [2004], using a similar zonal wind forcing in the subtropical upper stratosphere. We use the Reading Intermediate General Circulation Model (IGCM3), which

97 includes the troposphere, so that we can follow the response further down in the atmosphere and
98 also assess tropospheric signals. In addition, our model integrations include a seasonal cycle, while
99 Gray et al. [2004] modelled perpetual January conditions. The focus of our analysis will be on the
100 poleward and downward propagation of the response in the Northern Hemisphere (NH), and we
101 investigate how this propagation is affected by the representation of gravity wave effects in the
102 model.

103 Our study also builds on the work of Haigh et al. [2005] and Simpson et al. [2009] who investigated
104 the tropospheric response to temperature forcings in the lower stratosphere. They used a simplified
105 version of the model we use, with a lower top (at ~18.5 hPa compared to 0.1 hPa in our model) and
106 no orography, and hence very weak planetary wave activity. They could therefore not study the
107 downward propagation of the response to (an idealized) solar forcing from the upper stratosphere,
108 where the solar UV and stratospheric ozone interaction takes place, to the lower stratosphere. We
109 take their work a step further, by prescribing a forcing in the upper subtropical stratosphere. This
110 allows us to study the downward and poleward propagation of the responses within the
111 stratosphere as well as the responses in the troposphere. We stress that we purely focus on
112 dynamical propagation mechanisms, as do Haigh et al. [2005], Simpson et al. [2009] and Gray et al.
113 [2004]. As a second, but related point of interest, we examine the role of Stratospheric Sudden
114 Warming (SSW) events in the response that is produced. SSWs occur in response to strong planetary
115 wave forcings, which can cause a temporary breakdown of the winter polar vortex, with zonal winds
116 reversing to easterlies and a corresponding warming as a result. As planetary waves are also thought
117 to be involved in solar signal propagation, linkages between the occurrence of SSW events and the
118 poleward and downward transport of solar signals may be expected. Indeed, the modelling study by
119 Gray et al. [2004] already showed that a subtropical forcing in the upper stratosphere affects both
120 the timing and frequency of SSWs. Here we re-examine their results with a different model,
121 including seasonality and the option to use a gravity wave scheme. We also look at the link between

SSWs and solar forcing from another angle, by studying the effects of the absence/presence of SSWs on the responses obtained.

Both the sensitivities to gravity wave forcing and SSW occurrence that we find in the responses are used as a tool to gain insights in the dynamical mechanisms that are responsible for the poleward and downward propagation of the signal within the stratosphere, and for the communication of the signal from the stratosphere into the troposphere. In addition, by quantifying the sensitivity of the modelled responses to gravity wave effects and SSWs, we gain a better understanding of the importance of modelling these aspects of the stratospheric climate correctly. This helps to understand better why modelling studies so far have been unable to reproduce observed solar signals with the correct strength and timing, and informs future modelling studies that attempt a realistic simulation of solar cycle forcing.

2. IGCM3 description and experimental setup

2.1 IGCM3 description

The Reading Intermediate Global Circulation Model 3 (IGCM3) used in our experiments is a general circulation model based on the spectral dynamical core of Hoskins and Simmons [1975]. It accounts for a range of physical processes via parameterization schemes, as described in Forster et al. [2000]. These include a fast radiation scheme based on Morcrette [1990, 1991], a convection scheme based on Betts [1986], a boundary layer scheme based on Louis [1986], and a slab ocean and land surface scheme. In this sense, the IGCM3 is a general circulation model of intermediate complexity, bridging the gap between simple dynamical models and full state-of-the-art GCMs.

144 The model has been used extensively in radiative forcing studies [Forster et al., 2000, Joshi and
145 Shine, 2003, Shine et al., 2003]. More recently, improvements to the model were made for the
146 investigation of stratospheric processes and their effect on climate, in particular by providing a
147 realistic simulation of the stratospheric mean state and variability [Bell et al., 2009]. The dynamical
148 core of the model is the same as that of the model used by Haigh et al. [2005] and Simpson et al.
149 [2009] for studying solar effects.

150 For this study, a T42 horizontal resolution (triangular truncation at wavenumber 42) was used with
151 38 vertical levels from 1000 to 0.1 hPa (16 levels in the troposphere, 19 levels in the stratosphere,
152 and 3 levels above 1 hPa). Also, a gravity wave scheme was implemented, used for some of the
153 simulations. The gravity wave scheme is based on Lindzen [1981] and Holton [1982], as described by
154 Barnes [1990] and Joshi et al. [1995], and conserves momentum. It includes both orographic and
155 non-orographic waves.

156 The orographic waves are assumed to be stationary (phase speed = 0 m/s) and have an amplitude
157 based on the sub-grid scale standard deviation of the topography, with a minimum value of 100 m,
158 and the zonal wind speed at the surface. The mean orography from the US Naval 1/6th degree
159 resolution dataset is used. A minimum value of 100 m was set to parameterize roughly residual
160 breaking in the uppermost layers of the model of waves from slowly moving features (including over
161 oceans). Two types of non-orographic waves, with phase speeds equal to the zonal wind speed at
162 ~500 hPa +20 m/s and -20 m/s, respectively, and a fixed amplitude (a tuneable parameter) are
163 included. This is a simplified representation of non-orographic gravity waves compared to the much
164 larger spectrum of waves that is often included in full climate models extending up to the
165 mesosphere (e.g. Garcia et al., 2007). These spectra sometimes have a latitudinal and seasonal
166 dependence as well, while our two waves are distributed homogeneously in space and time,
167 although some temporal and spatial dependence in phase speed is caused through variations in
168 zonal wind speed at 500 hPa. Our simplified approach is justified for the following reasons. Firstly,

our model does not extend into the mesosphere, so that there is little gain in including waves with large phase speeds that would propagate through the stratosphere (and not break within the model domain). Secondly, Barnes (1990) notes that the overall impact of a relatively broad spectrum of waves on the zonal flow, even compared to just a single orographic mode, is not very large. And finally, the "true" spectrum of gravity waves, and their seasonal and latitudinal variation, remains not well known (e.g. Fritts and Alexander, 2003). Including more waves, with or without a latitudinally and seasonally varying source, would thus not necessarily make our simulations more realistic.

2.2 Experimental setup

Two control simulations were performed: one that used Rayleigh friction alone to account for gravity wave forcing, and another one that used the gravity wave parameterization. These will be referred to as RF-C and GWS-C, respectively. When only Rayleigh friction was used, this was employed over the top six model levels (~0.1-3 hPa) with a time scale of 18 days at the lowest level, reducing to a time scale of 3 days at the top level, over which winds were relaxed toward zero. The overall strength of the Rayleigh friction was chosen such that the zonal mean temperature and zonal wind climatologies for RF-C matched as closely as possible observed climatologies and the climatologies obtained with GWS-C. This excludes as much as possible the effects of different background climatologies on the response to the forcing. When the gravity wave scheme was used, a weak Rayleigh friction was still retained at the top four model levels (~0.1-1 hPa) with a time scale of 19 days at the lowest level reducing to 4.7 days at the top level, to avoid spurious wave reflections from the model top. The Rayleigh friction timescales for the RF and GWS simulations are shown in figure 1.

[[insert Figure 1 here]]

Two perturbed simulations were also performed and will be referred to as RF-P and GWS-P. The perturbation consisted of a relaxation of the zonal winds in the subtropical upper stratosphere over the top five model levels (~0.1-2 hPa), using a method similar to Rayleigh friction, but relaxing towards -20 m/s. The forcing was applied at a central latitude of 12.5° over a width of 17.5°, with a sinusoidal drop-off with latitude away from the central latitude, similar to that used by Gray et al. [2004]. The forcing was only switched on for the duration of 1 month (30 days) in April for the Southern Hemisphere (SH) and October for the Northern Hemisphere (NH), with a 10-day linear ramp up and down in the months before and after to make them smooth in time. These temporary forcings in early winter were chosen because forcing the model throughout the entire winter could make it difficult to separate forcing from response, and because the stratosphere appears to be particularly sensitive to solar perturbations originating from the subtropical upper stratosphere during early winter [Gray et al., 2001; Matthes et al., 2004]. All simulations were run for 50 years (18000 model days, with each month 30 days long for simplicity), in order to differentiate internal model variability from the true dynamic response to the applied perturbations.

We did not force the model directly by changing the incoming irradiance and ozone concentration (a seasonally varying ozone climatology based on Li and Shine [1995] was used in both control and perturbed simulations). However, by forcing the zonal winds, a corresponding temperature response in the forcing region is induced via thermal wind balance. The easterly forcing we apply acts to reduce the meridional temperature gradient, resulting in a cooling cell over the equator and a corresponding warming cell at higher latitudes. The structure of the forcing at 1-10 hPa is similar to observed solar signals in October-November [e.g. Frame and Gray, 2010]. For simplicity and to aid a straightforward explanation of the results, we assume the forced runs to represent solar minimum, and the control runs to represent solar maximum. This approach has also been followed by other studies investigating solar forcing effects, e.g. Gray et al. [2004]. The forcing we use results initially in a larger zonal wind anomaly than is observed to be associated with the solar cycle: the model gives a maximum zonal wind signal of 19 m/s during October, compared to 14 m/s in observations [Frame

and Gray, 2010]. However, this is justified, as our aim is not to reproduce solar signals exactly, but rather to investigate the relevant propagation mechanisms, and the influences of gravity wave effects and SSWs on the signal propagation.

3. Results

3.1 Control simulations

Figure 2 shows the October-November-December (OND) zonal mean temperature and zonal wind climatologies, together with their standard deviation (shaded), for the GWS-C (left) and RF-C (middle) simulations. The difference between the climatologies is also shown (right), with the shading now indicating statistical significance. The climatologies for the two simulations are very similar (which they were designed to be), and capture the main features of the observed zonal mean temperature and wind structures. There are statistically significant differences between the simulations, mainly in the stratosphere, but these differences are relatively small, and in particular the zonal wind in the NH polar vortex matches to a high degree.

[[insert Figure 2 here]]

The GWS-C simulation gives slightly stronger inter-annual variability, with standard deviations in temperature and zonal wind peaking at 3 K and 7 m/s, respectively, compared to 2.5 K and 5 m/s for RF-C. The distributions of SSW events for the two simulations were determined based on the criteria given in Charlton and Polvani [2007] and are shown in figure 3. They differ substantially, with the peak of the SSW distribution occurring 1-2 months earlier for RF-C than for GWS-C. The SSW distribution for GWS-C is in much better agreement with the observed distribution as reported by Charlton and Polvani [2007], in particular for December and January. Note that the higher standard

242 deviations found for GWS-C are not directly related to a higher occurrence frequency of SSW events.
243 Rather, the higher standard deviations for GWS-C may be related to a higher total wave activity in
244 that simulation, as expressed by EP fluxes and EP flux divergence. The EP fluxes and EP flux
245 divergence for the GWS-C simulation are approximately 25% larger in the NH upper stratosphere in
246 OND than for RF-C.

247 [[insert Figure 3 here]]

248 Both model simulations are lacking a Quasi-Biennial Oscillation (QBO) and a realistic semi-annual
249 oscillation (SAO). The zonal wind at 30-50 hPa in the equatorial regions, where the QBO is normally
250 defined, is permanently easterly. The model does produce an SAO-like oscillation, but this is biased
251 towards easterlies, so that the oscillation is between very weak easterlies at the equinoxes (0 m/s
252 for RF; 0 to -6 m/s for GWS) and stronger easterlies during the solstices (-8 m/s for RF; -12 to -14 m/s
253 for GWS) rather than between easterlies and westerlies, as in observations.

254

255 3.2 Perturbed-control differences

256 Figure 4 shows sequences of differences between the perturbed and control integrations for GWS in
257 zonal mean temperature (left) and zonal wind (right) for 10-day intervals from the start of November
258 to the start of December. The temperature signal clearly moves poleward and downward from Nov
259 1-10 to Nov 21-30, until it nearly vanishes in Dec 1-10. The zonal wind signal propagates in
260 conjunction with the temperature signal, and there is also a response present in the troposphere
261 throughout November, consisting of a strengthening of zonal winds at 40°N and a weakening at
262 60°N. This roughly maps on to the Northern Annular Mode (NAM; Thompson and Wallace, 1998],
263 although we note that the modelled zonal wind response to our forcing is shifted ~5° northward
264 compared to the NAM dipole pattern observed in observational data, and that also the modelled
265 tropospheric jet is located up to 5° further north than the observed jet.

[[insert Figure 4 here]]

The poleward and downward movement of the temperature and zonal wind responses in the stratosphere is dynamically consistent with the differences in EP flux and EP flux divergence, as shown in the left-hand panels of figure 5. The right-hand panels of figure 5 show the transformed Eulerian-mean [TEM; Andrews and McIntyre, 1976; Andrews et al., 1987] residual circulation, which is a measure of the large scale meridional circulation that is induced by wave forcing, i.e. the Brewer-Dobson (BD) circulation in the stratosphere.

[[insert Figure 5 here]]

In Nov 1-10 there is enhanced EP flux into the equator-ward flank of the polar vortex, and enhanced EP flux convergence (near 40°N, 1 hPa). This signifies an increase of the wave forcing on the mean flow, which acts to reduce the strength of the polar vortex. The enhanced wave forcing strengthens the BD circulation in the area below, with a corresponding weakening in the region above the enhanced wave forcing, effectively moving the circulation downwards. During Nov 11-20 and Nov 21-30, the upward EP flux into the polar vortex is further enhanced, while the centre of the activity moves poleward. As a result the polar vortex is gradually being weakened from the outside equator-ward flank to its inner core. The pair of positive and negative anomalies in the BD circulation also moves poleward (from ~15°N in Nov 1-10 to ~60°N in Nov 21-30), although the negative anomaly is no longer significant by Nov 21-30. In Dec 1-10 the system is recovering, but slightly overshooting, as the EP flux is now reduced and EP flux divergence is enhanced compared to the control run. The relatively weaker planetary wave forcing allows the polar vortex to strengthen again and weakens the high latitude branch of the BD circulation. After Dec 1-10 (not shown), there is very little significant signal remaining, indicating that the system has largely returned to its equilibrium state. This is in agreement with the observations of Lu et al. [2009] that the NH signals in the polar stratosphere have a life span of ~30-50 days, which is approximately the thermal relaxation timescale in the lower stratosphere [Newman and Rosenfield, 1997].

The responses obtained from the RF simulations are of similar strength and show similar spatial patterns in the stratosphere, but there are some differences in the timing of their poleward and downward propagation. The RF response moves noticeably quicker towards the pole, reaching the pole ~10 days earlier than the GWS response, with most of the downward propagation occurring after that time.

In the troposphere, significant responses in the zonal wind are detected, which are substantially different for RF and GWS, as shown in figure 6. There is relatively little movement of the tropospheric signal over time, and it is most significant for November. Therefore only an average response for November is shown. The zonal wind response for GWS consists of a weakening of the zonal flow at 10-20°N at 100-200 hPa, a strengthening throughout the depth of the troposphere centred at 40°N, and a weakening around 60°N at 250-500 hPa. This means that the core of the jet is strengthened (see figure 2 for the jet position in the control simulations). The RF zonal wind signal consists instead of a weakening from 15-20°N to 30-35°N through the depth of the troposphere and a slight strengthening around 50°N. This represents a poleward movement of the tropospheric jet. In both cases, the tropospheric responses do not appear to have directly descended from the stratosphere. They remain roughly in place throughout November-December, regardless of the temporal evolution of the stratospheric responses. At certain times they are therefore opposite in sign to the stratospheric responses.

[[insert figure 6 here]]

3.3 Effects on timing and frequency distribution of SSWs

Because the GWS-C simulation produced an SSW distribution that is in better agreement with observations than the RF-C simulation, the following sections will make use of the GWS results only. Figure 7 compares the SSW distributions for the forced and control simulations. The overall shape of

315 the SSW distribution remains the same, but the forced run shows a consistent increase in SSWs
316 throughout winter compared to the control runs. This is in agreement with the finding by Gray et al.
317 [2004] that the rest of the NH winter becomes more disturbed as a result of an easterly forcing in
318 early winter in the subtropical upper stratosphere. However, a change in the timing of SSWs, as
319 found by Gray et al. [2004], can not clearly be seen in our results.

320 [[insert figure 7 here]]

321

322 3.4 SSW effects on the responses

323 To investigate the influence of SSWs on the tropospheric responses to the forcing, we separated the
324 data for the forced and control GWS simulations in years with and without SSWs during OND. For
325 both simulations, 12 years with SSWs and 38 years without SSWs were identified (this included three
326 years with an October SSW for GWS-C, which were not shown in figure 7). As noted previously, the
327 zonal wind response in the troposphere resembles a NAM-like pattern. Therefore a NAM-like index
328 was calculated to show the difference in the temporal evolution of the signal between the non-SSW
329 and SSW datasets. This index was calculated by subtracting the area-weighted average of the
330 geopotential height for 40-60°N from the area-weighted average for 60-90°N. These latitude bands
331 were chosen specifically to capture the responses most clearly. The geopotential height difference
332 was then normalized by subtracting the mean climatology for the control and perturbed datasets,
333 and dividing the result by the standard deviation of the combined datasets. Positive values
334 correspond to a positive NAM phase and negative values to a negative NAM, although our index is
335 not directly comparable to the NAM due to the different latitude bands used. Figure 8 shows
336 pressure-time sections of the response in the normalized geopotential height difference between
337 60-90°N and 40-60°N for the datasets with and without SSWs.

For years with SSWs, stronger poleward propagation of the response to the forcing takes place in the stratosphere, so that the positive response in the stratospheric geopotential height difference occurs earlier and is stronger as well. However, the overall propagation pattern of a positive signal following a negative signal is similar for years with and without SSWs in the stratosphere. In contrast, in the troposphere we find a negative signal around Nov 10 that appears to have descended from the stratosphere for years with SSWs, while we find a signal of the opposite sign around the same time, and in fact throughout the whole time interval presented, when years with SSWs are excluded. The non-SSW tropospheric response does not appear directly connected to the stratospheric response. When the entire dataset (SSW + non-SSW years) is processed, the signal around Nov 10 is weaker, while the signal around Nov 20 is stronger. The signals from the two conditions thus act to cancel each other out partly around Nov 10, while they add up around Nov 20.

[[insert figure 8 here]]

4. Discussion

4.1 Influences of gravity wave effects on solar signal propagation

Previous modelling studies have demonstrated that the representation of the stratosphere in a general circulation model can influence the troposphere [e.g. Boville, 1984; Song and Robinson, 2004; Sigmond et al., 2008]. Here we build on those findings and show a specific influence of the representation of gravity wave effects on the downward and poleward propagation of an idealized solar forcing in the upper stratosphere. Differences between the GWS and RF simulations occur in terms of the timing and extent of poleward and downward propagation of the responses in the stratosphere, and also in general in the responses in the troposphere, even though the differences between the RF and GWS simulations in terms of forcing and gravity wave representation are in the

362 (upper) stratosphere. The influences we find in the lower stratosphere and troposphere are thus
363 indirect.

364 The tropospheric zonal wind response for GWS is to some extent in agreement with observations by
365 Haigh et al. [2005], who found that the tropospheric jets are weaker and shift polewards for higher
366 solar activity. The GWS results did not show the change in jet position, but did show a change in
367 strength in the same sense, bearing in mind that our results are presented as solar minimum-
368 maximum conditions. The RF results on the other hand showed mostly a change in jet position, but it
369 moved poleward for solar minimum conditions compared to solar maximum, i.e. in the opposite
370 sense to the observations by Haigh et al. [2005]. For both RF and GWS the strength of the
371 tropospheric zonal wind signal is comparable to the strength of the observed anomalies reported by
372 Haigh et al., [2005]. The GWS pattern of a strengthening of the jet at 40°N with a weakening on
373 either side also matches the general pattern of the zonal wind signal observed by Frame and Gray
374 [2010], although their pattern is centred at 30-35°N, while the RF pattern does not. The GWS
375 simulations thus give a more realistic tropospheric response, in better agreement with observations.

376 Sigmond and Scinocca [2010] found that the sensitivity of the doubled CO_2 response to
377 parameterized orographic gravity wave drag [Sigmond et al., 2008] was largely due to differences in
378 the control climatologies. In our case, the differences in response to an idealized solar forcing do not
379 seem to be related to such differences, as the control climatologies were designed to be similar. We
380 can also exclude the possibility that the differences are related to different distributions of SSW
381 events (which were shown to differ more substantially), as excluding years with SSW events in OND
382 did not result in better agreement between the RF and GWS responses in OND (results not shown).
383 Shibata and Kodera [2005] interpreted the differences in response they found between their model
384 versions with Rayleigh friction and the Hines parameterization scheme in terms of the
385 absence/presence of an SAO. In our simulations however, we do not get a realistic SAO in either the

386 RF or GWS simulations. Therefore, while the SAO may have an influence in reality, it is not the
387 reason for the differences we find in our results. We will now explore two alternative explanations.

388 Firstly, it may be possible that the gravity wave forcing itself played a role in the propagation and
389 maintenance of the signal, by redistributing gravity wave momentum deposition, similar to how
390 planetary waves are thought to play a role in signal propagation by redistributing their momentum
391 deposition. We therefore examined the difference in gravity wave-induced accelerations between
392 the forced and control GWS runs, which revealed that these always acted to reduce the zonal wind
393 responses found (results not shown). So rather than amplifying the response, the direct effects of
394 changes in gravity wave momentum deposition acted to diminish the response, and we can
395 eliminate this possibility.

396 A second pathway for gravity wave effects to influence the response to our forcing is through
397 indirect effects on planetary waves. As noted, the EP fluxes and EP flux divergence were about 25%
398 larger in the NH upper stratosphere during OND for GWS-C compared to RF-C. This is consistent with
399 the finding by McLandress and McFarlane [1993] that longitudinal variations in gravity wave drag
400 (which would be missing in a Rayleigh friction approach) can enhance planetary wave amplitudes
401 and EP flux divergence. Considering the mechanism proposed by Kodera and Kuroda [2002], this
402 could explain why the stratospheric responses propagate differently for the GWS and RF versions of
403 the model, although the detail of the differences is not straightforward to explain.

404 The stronger planetary wave activity may also be responsible for the slightly stronger inter-annual
405 variability found for GWS. However, this small enhancement in inter-annual variability is not
406 sufficient to determine whether a lack of inter-annual variability is responsible for a too weak
407 response to solar forcing, as suggested by Matthes et al. [2004] and Kodera et al. [2003]. In terms of
408 strength, the responses obtained with the RF and GWS versions of the model are very similar.

In conclusion, our results indicate that it is important to model the planetary wave activity correctly, and as gravity wave effects can modify this activity substantially, a more realistic representation of gravity wave effects seems to be necessary to achieve this. The use of a gravity wave scheme does not only affect stratospheric responses, but also the responses in the troposphere, which become more realistic when the gravity wave scheme is used. We note that our model simulations, despite making use of a gravity wave scheme, still do not necessarily provide a realistic description of gravity wave effects, as strong assumptions were made on the characteristics of the waves. However, more information on the global distribution of gravity wave effects is becoming available now [e.g. Alexander et al., 2008] and future studies that attempt to realistically model the response to solar forcing should take advantage of this.

4.2 Influences of SSW events on solar signals

Separating our data into years with and without SSW events in OND showed that responses are substantially different under both conditions. Years with SSWs are highly disturbed, and typically have a strong planetary wave forcing in the high latitude upper stratosphere, causing the polar vortex to break down. Again, considering the Kodera and Kuroda [2002] mechanism of solar signal propagation, we would expect poleward and downward propagation to be enhanced under such conditions, and that is indeed what we observe. During years with SSWs a negative stratospheric signal appears to descend down into the troposphere directly, becoming strongest there around Nov 10. This is followed by a positive stratospheric response, which also appears to descend down, although the tropospheric response, while positive also, is not significant. In contrast, when years with SSWs are excluded, the tropospheric signals are positive throughout and do not change in conjunction with the time-varying changes in the stratosphere. The tropospheric signals appear therefore more disconnected from the stratospheric signals in this case.

433 This does not mean that there is no connection between the phase of the NAM in the troposphere
434 and stratosphere when no SSWs are present, but suggests that different types of troposphere-
435 stratosphere coupling are dominant for disturbed (with SSWs) and quiet (no SSWs) conditions. The
436 mechanism responsible for the non-SSW signals is unlikely to be a direct tropospheric extension of
437 the mechanism responsible for the poleward and downward propagation of the stratospheric
438 signals. In other words, those tropospheric signals do not appear to be due to a change in planetary
439 wave forcing, and an associated change in a mean meridional circulation, extending from the
440 stratosphere into the troposphere, as this should have resulted in signals of the same sign in both
441 the stratosphere and troposphere. We therefore discuss two alternative coupling mechanisms.

442 The first mechanism involves changes in the tropospheric mean meridional circulation, forced by
443 changes in eddy momentum fluxes associated with synoptic waves within the troposphere [Simpson
444 et al., 2009]. The changes in eddy momentum fluxes are brought about by changes in temperature
445 gradients and zonal wind accelerations at the tropopause, in response to changes in the lower
446 stratospheric temperature structure and flow. Simpson et al. [2009] demonstrated the above
447 mechanism by modelling the effect of an altered latitudinal temperature structure in the lower
448 stratosphere on the troposphere. They showed that the response slowly develops in the upper
449 troposphere, over about 10 days, and gradually spreads to the lower troposphere, with the main
450 response structure established after about 20 days.

451 In our results we do not see a clear downward movement of the signal from the upper troposphere
452 into the lower troposphere over time, even though our model is a more advanced version of the
453 model used by Simpson et al. [2009]. Also, in our experiments the stratospheric signal does not
454 penetrate down into the lower stratosphere when years with SSWs are excluded, while there is still
455 a clear tropospheric response. It is therefore unlikely that the above mechanism is responsible for
456 our tropospheric response, although it is still possible that tropospheric eddies are involved in

457 amplifying/maintaining the tropospheric response (see also Kushner and Polvani, 2004; Song and
458 Robinson, 2004], once initiated by some other process.

459 The second mechanism involves changes in the reflection of planetary waves by the stratosphere
460 back into the troposphere, where they are subsequently absorbed [Perlwitz and Harnik, 2003, 2004;
461 Shaw et al., 2010]. Perlwitz and Harnik [2004] argued that this mechanism becomes more important
462 when the polar vortex is strong, in particular the lower part of the vortex (~30 hPa), as more wave
463 activity in that case is reflected back into the troposphere, rather than being absorbed by the
464 stratosphere. They also found that it is important mainly on short timescales (up to 12 days).

465 This mechanism could potentially explain why we find a different tropospheric signal for years with
466 and without SSWs. During years with SSWs, troposphere-stratosphere coupling via reflection of
467 planetary waves would be weak, while the mechanism would be more important, resulting in
468 stronger coupling, during years without SSWs, when the polar vortex is stronger. This is consistent
469 with our finding that tropospheric signals of opposite sign appear or become enhanced for years
470 without SSWs, while no significant signal, or a signal with the same sign as that in the stratosphere
471 appears for years with SSWs.

472 Previous studies have shown that there is a strong coupling between the troposphere and
473 stratosphere associated with SSWs [Baldwin and Dunkerton, 2001; Charlton and Polvani, 2007], but
474 this appears to be a more direct coupling, with signals from the stratosphere apparently descending
475 down into the troposphere. This is indeed what we observe in our results with SSWs, although most
476 of the responses are not significant. This could be due to the fact that the datasets with SSWs are
477 much shorter than the datasets without SSWs, and within the SSW datasets the SSWs also occurred
478 at different times. This gives a noisier dataset and makes it harder to establish a significant response.
479 A second possibility is that our forcing during years with SSWs could be relatively less important to
480 the troposphere than it is during years without SSWs, due to the dominance of the SSW influence on
481 the troposphere-stratosphere coupling in years with SSWs.

Finally, we note that the tropospheric responses of the SSW and non-SSW are sometimes of the opposite sign and can therefore act to cancel each other out. This could be a possible reason for difficulties in establishing a significant tropospheric signal in observational data, as both disturbed and undisturbed years are normally included.

4.3 QBO influences

The interaction between the QBO and solar forcing is still unclear. Some studies have found that solar forcing influences the QBO [McCormack et al., 2007] or that the QBO affects solar signals [Labitzke and Van Loon, 1988; Gray et al., 2004; Labitzke et al., 2006], while others find little interaction [Austin et al., 2008]. Lu et al. [2009] and Ito et al. [2009] found that the effects of the QBO on solar signal propagation occur predominantly in late winter.

Our results were obtained with permanently weak easterlies in the equatorial stratosphere, so that any interactions between solar forcing and the QBO have not been considered. However, as we focus on early winter, the absence of a QBO may not have had a large effect. Still, the QBO affects the distribution of planetary wave activity, which plays a key role in the poleward and downward propagation of the signal in the stratosphere. Inclusion of a realistic QBO could therefore in principle modify our results somewhat. On a background of westerly winds in the equatorial stratosphere, an easterly forcing should still have the effect of deflecting waves poleward, but the strength of the signal and the timing and extent of poleward propagation might be different.

5. Summary and conclusions

Our results broadly confirm the mechanism for solar signal propagation in the stratosphere proposed by Kodera and Kuroda [2002]. We find that, in agreement with their theory, the redistribution of planetary wave activity can strengthen an initial forced signal, and transport it polewards and downwards from the equatorial upper stratosphere. We find that the type of representation of gravity wave effects in our model influences this process, changing the timing and extent of poleward and downward signal propagation in the stratosphere. This takes place most likely through indirect effects of gravity wave-induced accelerations on planetary waves. The results obtained with the gravity wave scheme are more realistic than those obtained with Rayleigh friction, as they are in better agreement with observed solar signals, in particular in the troposphere.

The GWS results also produce a more realistic distribution of SSW events. The absence/presence of SSW events has an effect on the propagation of the response to our forcing, mainly in the troposphere. For years with SSWs tropospheric signals appear to descend directly from the stratosphere, while they appear more disconnected when SSW years are excluded. We suggest that this is due to different types of troposphere-stratosphere coupling being active under conditions with and without SSWs. Under quiet conditions, a signal in the troposphere of the opposite sign to that in the stratosphere may be generated through small modifications in the reflection of planetary waves back into the troposphere. Once initiated, this signal may be maintained and/or strengthened locally through changes in eddy momentum fluxes. In contrast, under disturbed conditions, when SSWs occur, the troposphere-stratosphere coupling occurs more directly, and the tropospheric response is an extension of that in the stratosphere.

The forcing also increases the number of SSWs, but does not influence their timing, as found by Gray et al. [2004]. We therefore confirm only part of the findings of Gray et al. [2004]. Their result that earlier SSWs occurred when an easterly forcing in the subtropical upper stratosphere was applied may have been related to the absence of a seasonal cycle in their model integrations.

Acknowledgements

We are very grateful to three anonymous reviewers for their constructive comments, which helped to improve the original manuscript.

References

Alexander, M.J., J. Gille, C. Cavanaugh, M. Coffey, C. Craig, T. Eden, G. Francis, C. Halvorson, J. Hannigan, R. Khosravi, D. Kinnison, H. Lee, S. Massie, B. Nardi, J. Barnett, C. Hepplewhite, A. Lambert and V. Dean (2008). Global estimates of gravity wave momentum flux from High Resolution Dynamics Limb Sounder observations, *J. Geophys. Res., 113*(D15), D15S18.

Andrews, D.G., J.R. Holton and C.B. Leovy, 1987. *Middle atmosphere dynamics,* pp. 489, Academic Press, London, UK.

Andrews, D.G. and M.E. McIntyre (1976). Planetary waves on horizontal and vertical shear: the generalized Eliassen-Palm Relation and the mean zonal acceleration, *J. Atmos. Sci., 33*(11), 2031-2048.

Austin, J., K. Tourpali, E. Rozanov, H. Akiyoshi, S. Bekki, G. Bodeker, C. Brühl, N. Butchart, M. Chipperfield, M. Deushi, V.I. Fomichev, M.A. Giorgetta, L. Gray, K. Kodera, F. Lott, E. Manzini, D. Marsh, K. Matthes, T. Nagashima, K. Shibata, R.S. Stolarski, H. Struthers and W. Tian (2008). Coupled chemistry climate model simulations of the solar cycle in ozone and temperature, *J. Geophys. Res., 113*(D11), D11306, doi: 10.1029/2007JD009391.

Baldwin, M.P. and T.J. Dunkerton (2001). Stratospheric harbingers of anomalous weather regimes, *Science, 294*(5542), 581-584.

551 Barnes, J.R. (1990). Possible effects of breaking gravity waves on the circulation of the middle
552 atmosphere of Mars, *J. Geophys. Res., 95*(B2), 1401-1421.

553 Bell, C.J., L.J. Gray, A.J. Charlton-Perez and M.M. Joshi (2009). Stratospheric cimmunication of El Niño
554 teleconnections to European winter, *J. Clim., 22*(15), 4083-4096. doi:10.1175/2009JCLI2717.1.

555 Betts, A.K. (1986). A new convective adjustment scheme 1. Observational and theoretical basis, *Q. J.*
556 *R. Meteorol. Soc., 112*(473), 677-691.

557 Boville, B.A. (1984), The influence of the polar night jet on the tropospheric circulation in a GCM, *J.*
558 *Atmos. Sci., 41*(7), 1132-1142.

559 Charlton, A.J. and L.M. Polvani (2007). A new look at Stratospheric Sudden Warmings. Part 1:
560 Climatology and modelling benchmarks, *J. Clim., 20*(3), 449-469.

561 Cnossen, I., M.J. Harris, N.F. Arnold and E. Yigit (2009). Modelled effect of changes in the CO_2
562 concentration on the middle and upper atmosphere: Sensitivity to gravity wave parameterization, *J.*
563 *Atmos. Solar-Terr. Phys., 71*(13), 1484-1496. doi:10.1016/j.jastp.2008.09.014.

564 Crooks, S.A. and L.J. Gray (2005). Characterization of the 11-year solar signal using a multiple
565 regression analysis of the ERA-40 dataset, *J. Clim., 18*(7), 996-1015.

566 Dunkerton, T.J. (1982). Stochastic parameterization of gravity wave stresses, *J. Atmos. Sci., 39*(8),
567 1711-1725.

568 Forster, P.M., M. Blackburn, R. Glover and K.P. Shine (2000). An examination of climate sensitivity for
569 idealised climate change experiments in an intermediate general circulation model, *Clim. Dyn.,*
570 *16*(10-11), 833-849.

571 Frame, T.H.A. and L.J. Gray (in press, 2010). The 11-year solar cycle in ERA-40 data: an update to
572 2008, *J. Clim., xx*(xx), xx-xx.

573 Fritts, D.C. and M.J. Alexander (2003). Gravity wave dynamics and effects in the middle atmosphere,
574 *Rev. Geophys., 41*(1), 1003.

575 Gray, L.J., J. Beer, M. Geller, J.D. Haigh, M. Lockwood, K. Matthes, U. Cubasch, D. Fleitmann, G.
576 Harrison, L. Hood, J. Luterbacher, G. Meehl, D. Shindell, B. van Geel and W. White (2010, in press).
577 Solar influences on climate, *Rev. Geophys., xx*(xx), xx-xx.

578 Gray, L.J., S. Crooks, C. Pascoe, S. Sparrow and M. Palmer (2004). Solar and QBO influences on the
579 timing of stratospheric sudden warmings, *J. Atmos. Sci., 61*(23), 2777-2796.

580 Gray, L.J., S.J. Phipps, T.J. Dunkerton, M.P. Baldwin, E.F. Drysdale and M.R. Allen (2001). A data study
581 of the influence of the equatorial upper stratosphere on northern-hemisphere stratospheric sudden
582 warmings, *Q. J. R. Meteorol. Soc. 127*(576), 1985-2003.

583 Gray, L.J., S.T. Rumbold and K.P. Shine (2009). Stratospheric temperature and radiative forcing
584 response to 11-year solar cycle changes in irradiance and ozone, *J. Atmos. Sci., 66*(8), 2402-2417.

585 Gray, L.J., S. Sparrow, M. Juckes, A. O'Neill and D.G. Andrews (2003). Flow regimes in the winter
586 stratosphere of the northern hemisphere, *Q. J. R. Meteorol. Soc.129*(589), 925-945.

587 Haigh, J.D. (1996). The impact of solar variability on climate, *Science, 272*(5264), 981-984.

588 Haigh, J.D. (1994). The role of stratospheric ozone in modulating the solar radiative forcing of
589 climate, *Nature, 370*(6490), 544-546.

590 Haigh, J.D., M. Blackburn and R. Day (2005). The response of the tropospheric circulation to
591 perturbations in lower-stratospheric temperature, *J. Clim., 18*(17), 3672-3685.

592 Hines, C.O. (1997). Doppler-spread parameterization of gravity-wave momentum deposition in the
593 middle atmosphere. Part 1: Basic formulation, *J. Atmos. Solar-Terr. Phys., 59*(4), 371-386.

594 Holton, J.R. (1982). The role of gravity wave induced drag and diffusion in the momentum budget of
595 the mesosphere, *39*(4), 791-799.

596 Hood, L.L., 2004. Effects of solar UV variability on the stratosphere, in *Solar variability and its effects*
597 *on climate*, edited by Pap, J.M. and P. Fox, pp. 283-303, American Geophysical Union, Washington
598 DC, USA.

599 Joshi, M.M. and K.P. Shine (2003). A GCM study of volcanic eruptions as a cause of increased
600 stratospheric water vapor, *J. Clim., 16*(21), 3525-3534.

601 Joshi M.M., B.N. Lawrence and S.R. Lewis (1995). Gravity wave drag in 3D atmospheric models of
602 Mars*, J. Geophys. Res., 100*(E10), 21235-21245.

603 Hood, L.L., J.L. Jirikowic and J.P. McCormack (1993). Quasi-decadal variability of the stratosphere:
604 influence of long-term solar ultraviolet variations, *J. Atmos. Sci., 50*(24), 3941-3958.

605 Hoskins, B.J. and A.J. Simmons (1975). A multi-layer spectral model and the semi-implicit method, *Q.*
606 *J. R. Meteorol. Soc., 101*(429), 637-655.

607 Ito, K., Y. Naito, and S. Yoden (2009), Combined effects of QBO and 11-year solar cycle on the winter
608 hemisphere in a stratosphere-troposphere coupled system, *Geophys. Res. Lett.*, 36, L11804,
609 doi:10.1029/2008GL037117.

610 Kodera, K. and Y. Kuroda (2002). Dynamical response to the solar cycle, *J. Geophys. Res., 107*(D24),
611 4749.

612 Kodera, K., K. Matthes, K. Shibata, U. Langematz and Y. Kuroda (2003). Solar impact on the lower
613 mesospheric subtropical jet: a comparative study with general circulation model simulations,
614 *Geophys. Res. Lett., 30*(6), 1315. doi:10.1029/2002GL016124.

615 Kushner, P.J. and L.M. Polvani (2004). Stratosphere-troposphere coupling in a relatively simple
616 AGCM: The role of eddies, *J. Clim., 17*(3), 629-639.

617 Labitzke, K. and H. Loon van (1988). Associations between the 11-year solar cycle, the QBO and the
618 atmosphere 1. The troposphere and stratosphere on the Northern Hemisphere in winter, *J. Atmos.*
619 *Terr. Phys., 50*(3), 197-206.

620 Labitzke, K, M. Kunze, and S. Bronnimann (2006). Sunspots, the QBO and the stratosphere in the
621 North Polar Region - 20 years later, *Meteorol. Zeitschrift*, 15, 355-363.

622 Li, D. and K.P. Shine (1995). A 4-dimensional ozone climatology for UGAMP models, *UGAMP Internal*
623 *Report, 35*.

624 Lindzen, R.S. (1981). Turbulence and stress owing to gravity wave and tidal breakdown, *J. Geophys.*
625 *Res., 86*(NC10), 9707-9714.

626 Louis, J.F., 1986. *Forecast model research manual 3: physical parameterization,* European Centre for
627 Medium Range Weather Forecasts, Research Department, Reading UK.

628 Lu, H., L.J. Gray, M.P. Baldwin and M.J. Jarvis (2009). Life cycle of the QBO-modulated 11-year solar
629 cycle signals in the Northern Hemispheric winter, *Q. J. R. Meteorol. Soc., 135*(641), 1030-1043.
630 doi:10.1002/qj.419.

631 Marsh, D.R., R.R. Garcia, D.E. Kinnison, B.A. Boville, F. Sassi, S.C. Solomon and K. Matthes (2007).
632 Modeling the whole atmosphere response to solar cycle changes in radiative and geomagnetic
633 forcing, *J. Geophys. Res., 112*(D23), D23306, doi:10.1029/2006JD008306.

634 Matthes, K., Y. Kuroda, K. Kodera and U. Langematz (2006). Transfer of the solar signal from the
635 stratosphere to the troposphere: Northern winter, *J. Geophys. Res., 111*(D6), D06108.
636 doi:10.1029/2005JD006283.

637 Matthes, K., U. Langematz, L.J. Gray, K. Kodera and K. Labitzke (2004). Improved 11-year solar signal
638 in the Freie Universität Berlin Climate Middle Atmosphere Model (FUB-CMAM), *J. Geophys. Res.,*
639 *109*(D6), D06101. doi:10.1029/2003JD004012.

640 McCormack, J.P., D.E. Siskind and L.L. Hood (2007). Solar-QBO interaction and its impact on
641 stratospheric ozone in a zonally averaged photochemical transport model of the middle atmosphere,
642 *J. Geophys. Res., 112*(D16), D16109. doi:10.1029/2006JD008369.

643 McLandress, C. and N.A. McFarlane (1993). Interactions between orographic gravity wave drag and
644 forced stationary planetary waves in the winter Nortern Hemisphere middle atmosphere, *J. Atmos.*
645 *Sci., 50*(13), 1966-1990.

646 Morcrette, J.J. (1991). Radiation and cloud radiative properties in the European Centre for Medium
647 Range Weather Forecasts forecasting system, *J. Geophys. Res., 96*(D5), 9121-9132.

648 Morcrette, J.J. (1990). Impact of changes to the radiation transfer parameterizations plus cloud
649 optical properties in the ECMWF model, *Mon. Weather Rev., 118*(4), 847-873.

650 Newman, P.A. and J.E. Rosenfield (1997). Stratospheric thermal damping times, *Geophys. Res. Lett.,*
651 *24*(4), 433-436.

652 Perlwitz, J. and N. Harnik (2004). Downward coupling between the stratosphere and troposphere:
653 the relative role of wave and zonal mean processes, *J. Clim., 17*(24), 4902-4909.

654 Perlwitz, J. and N. Harnik (2003). Observational evidence of a stratospheric influence on the
655 troposphere by planetary wave reflection, *J. Clim., 16*(18), 3011-3026.

Shaw, T.A., J. Perlwitz and N. Harnik (submitted, 2010). Downward wave coupling between the stratosphere and troposphere: the importance of meridional wave guiding and comparison with zonal-mean coupling, *J. Clim., xx*(xx), xx-xx.

Shepherd, T.G., K. Semeniuk and J.N. Koshyk (1996). Sponge layer feedbacks in middle-atmosphere models, *J. Geophys. Res., 101*(D18), 23447-23464.

Shepherd, T.G. and T.A. Shaw (2004). The angular momentum constraint on climate sensitivity and downward influence in the middle atmosphere, *J. Atmos. Sci., 61*(23), 2899-2908.

Shibata, K. and K. Kodera (2005). Simulation of radiative and dynamical responses of the middle atmosphere to the 11-year solar cycle, *J. Atmos. Solar-Terr. Phys., 67*(1-2), 125-143. doi:10.1016/j.jastp.2004.07.022.

Shine, K.P., J. Cook, E.J. Highwood and M.M. Joshi (2003). An alternative to radiative forcing for estimating the relative importance of climate change mechanisms, *Geophys. Res. Lett., 30*(20), 2047. doi: 10.1029/2003GL018141.

Sigmond, M. and J.F. Scinocca (2010). The influence of the basic state on the Northern Hemisphere circulation response to climate change, *J. Clim., 23*(6), 1434-1446. doi:10.1175/2009JCLI3167.1.

Sigmond, M., J.F. Scinocca and P.J. Kushner (2008). Impacts of the stratosphere on tropospheric climate change, *Geophys. Res. Lett., 35*(12), L03704. doi:10.1029/2008GL033573.

Simpson, I.R., M. Blackburn and J.D. Haigh (2009). The role of eddies in driving the tropospheric response to stratospheric heating perturbations, *J. Atmos. Sci., 66*(5), 1347-1365. doi:10.1175/2008JAS2758.1.

Song, Y. and W.R. Robinson (2004). Dynamical mechanisms for stratospheric influences on the troposphere, *J. Atmos. Sci., 61*(14), 1711-1725.

678 Thompson, D.W.J. and J.M. Wallace (1998). The Arctic Oscillation signature in the wintertime
679 geopotential height and temperature fields, *Geophys. Res. Lett., 25*(9), 1297-1300.

680

681 **Figure captions**

682 Figure 1. Rayleigh friction timescales used for the top levels of the RF and GWS simulations.

683 Figure 2. Zonal mean temperature (top) and zonal wind (bottom) climatologies for the GWS-C
684 simulation (left), the RF-C simulation (middle), and the difference between the GWS-C and RF-C
685 simulations (right) for OND. For the left and middle panels the shading indicates the standard
686 deviation. For the right panels the shading indicates statistical significance at the 95% (light shading)
687 and 99% (dark shading) level, as determined with a T-test.

688 Figure 3. Distribution of the occurrence frequency of SSW events for the RF-C and GWS-C
689 simulations and the observed SSW frequency from Charlton and Polvani (2007) based on the
690 average of the NCEP and ERA-40 occurrences.

691 Figure 4. Differences in the zonal mean temperature (left) and zonal wind (right) climatologies
692 between the GWS perturbed and control simulations for 10-day averages from Nov 1-10 to Dec 1-
693 10. Light shading indicates 95% statistical significance, and dark shading 99% statistical significance,
694 as determined with a T-test.

695 Figure 5. Differences in the EP flux (arrows) and EP flux divergence (contours; left), scaled according
696 to the "acceleration" scaling defined by Gray et al. [2003], and TEM flow vectors (arrows) and
697 residual circulation (contours; right) climatologies between the GWS perturbed and control
698 simulations for 10-day averages from Nov 1-10 to Dec 1-10. EP flux vectors have units of m^2s^{-2}, with
699 a metric factor applied to give reasonable arrow lengths on the plot, and the EP flux divergence has
700 units of $ms^{-1}day^{-1}$. The TEM residual circulation has units of 10^9 kg/s and is scaled by $1/\sigma$, where σ =

$P/P_{surface}$, the TEM horizontal flow vector has units of ms^{-1}, and the TEM vertical flow vector has units of mb $hour^{-1}$ and is also scaled by 1/σ. A metric factor is applied to the flow vectors to give reasonable arrow lengths on the plot. Light shading indicates 95% statistical significance, and dark shading 99% statistical significance, as determined with a T-test.

Figure 6. Differences in the zonal mean zonal wind climatologies in the troposphere for the perturbed and control simulations for GWS (left) and RF (right) for November. Light shading indicates 95% statistical significance, and dark shading 99% statistical significance, as determined with a T-test.

Figure 7. Distribution of the occurrence frequency of SSW events for the GWS for the control and perturbed simulations.

Figure 8. Pressure-time section of the normalized geopotential difference between 60-90°N and 40-60°N between the GWS perturbed and control datasets without SSWs (left) and with SSWs (right) from Oct 10 to Dec 30. There are 12 years with SSWs and 38 years without SSWs in both GWS-C and GWS-P. Light shading indicates 90% statistical significance, and dark shading 95% statistical significance, as determined with a T-test.

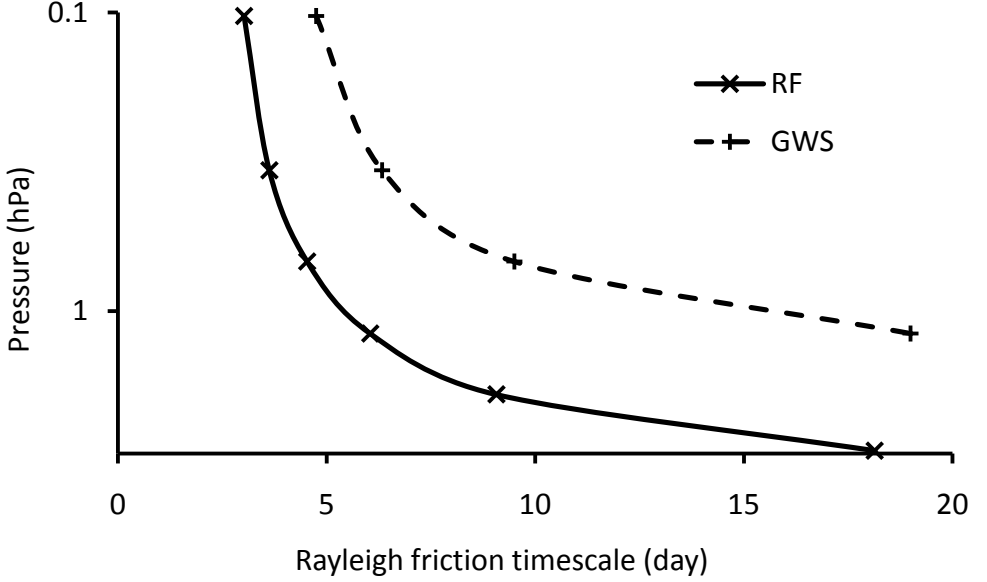
0.1
1
Pressure (hPa)
RF
GWS
0
5
10
15
20
Rayleigh friction timescale (day)

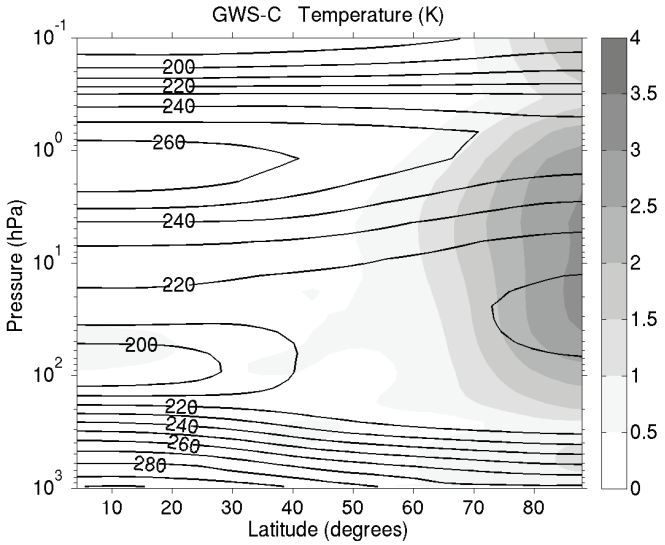
GWS-C Temperature (K)
Pressure (hPa)
Latitude (degrees)

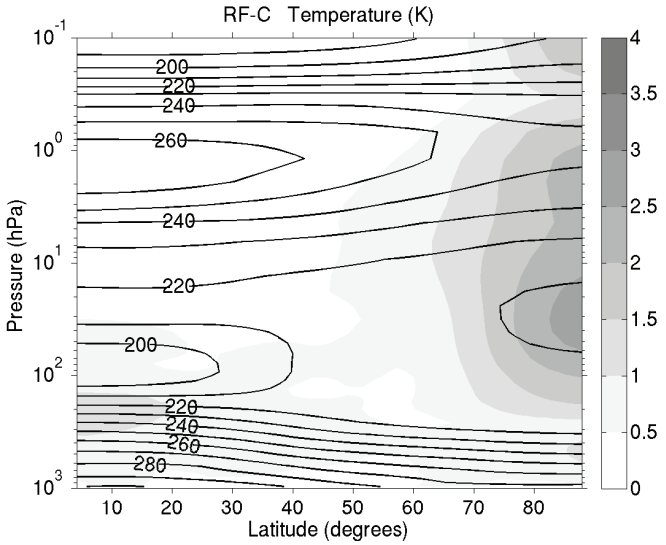
RF-C Temperature (K)
Pressure (hPa)
Latitude (degrees)

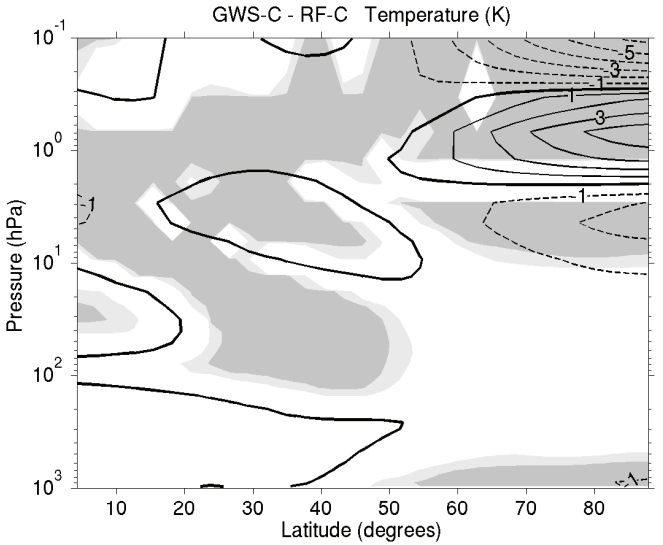
GWS-C - RF-C Temperature (K)
Pressure (hPa)
Latitude (degrees)

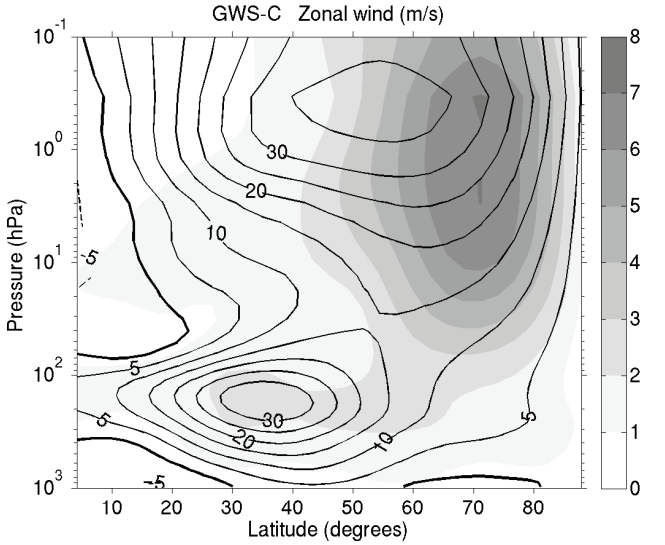
GWS-C Zonal wind (m/s)
Pressure (hPa)
Latitude (degrees)

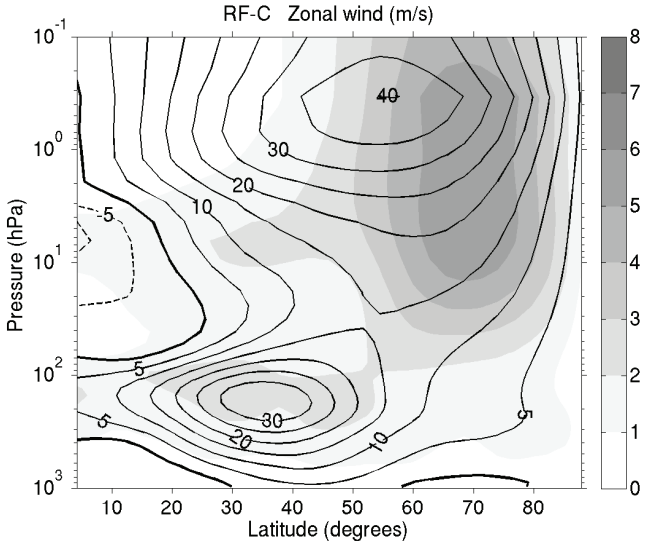
RF-C Zonal wind (m/s)
Pressure (hPa)
Latitude (degrees)

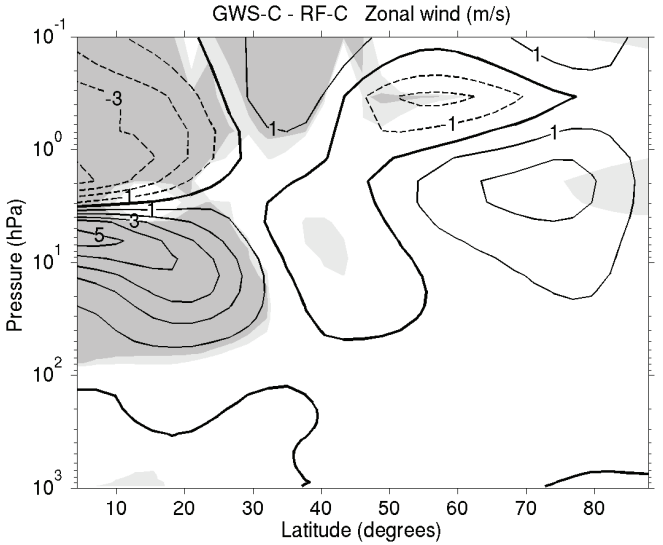
GWS-C - RF-C Zonal wind (m/s)
Pressure (hPa)
Latitude (degrees)

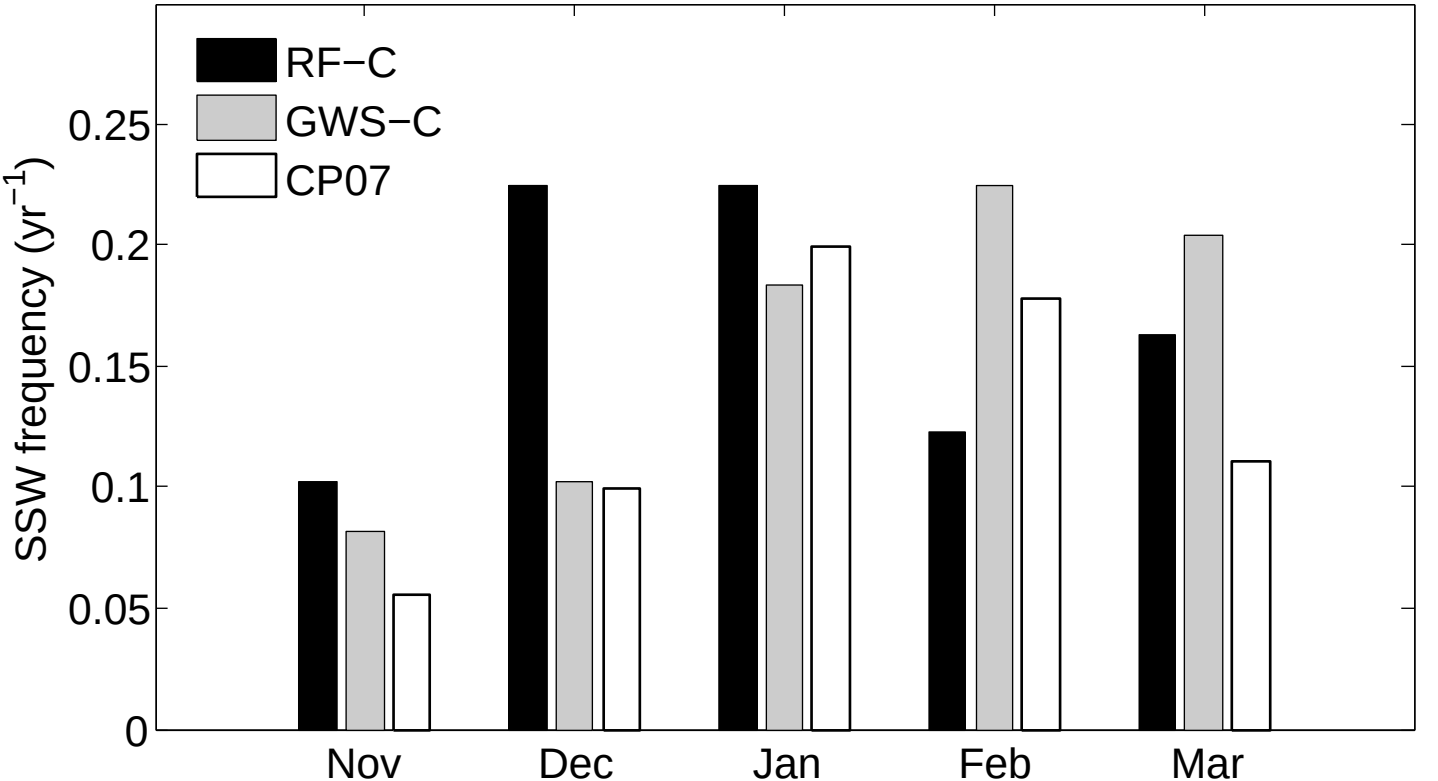
RF−C
GWS−C
CP07
SSW frequency (yr^{-1})
0
0.05
0.1
0.15
0.2
0.25
Nov
Dec
Jan
Feb
Mar

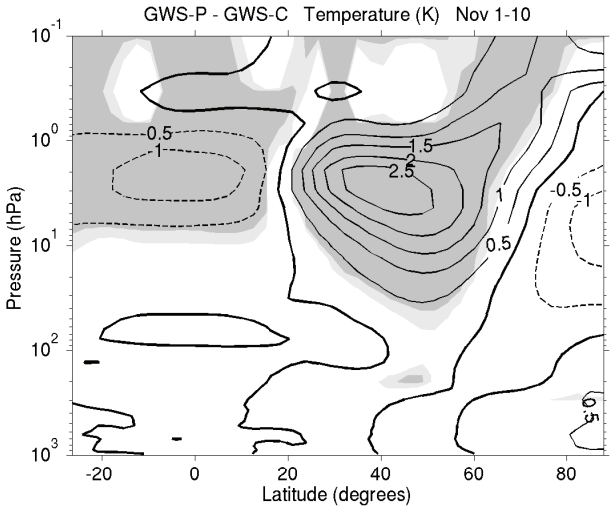
GWS-P - GWS-C Temperature (K) Nov 1-10
Pressure (hPa)
Latitude (degrees)

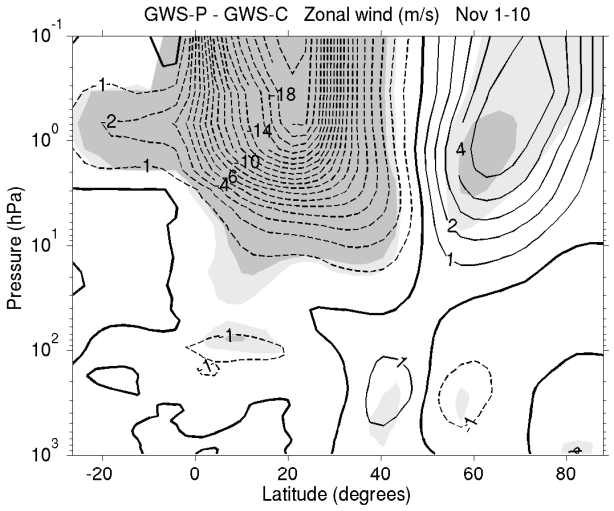
GWS-P - GWS-C Zonal wind (m/s) Nov 1-10
Pressure (hPa)
Latitude (degrees)

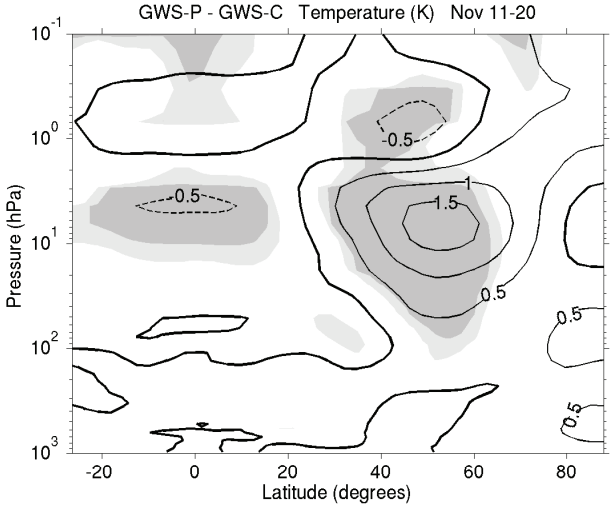
GWS-P - GWS-C Temperature (K) Nov 11-20
Pressure (hPa)
Latitude (degrees)

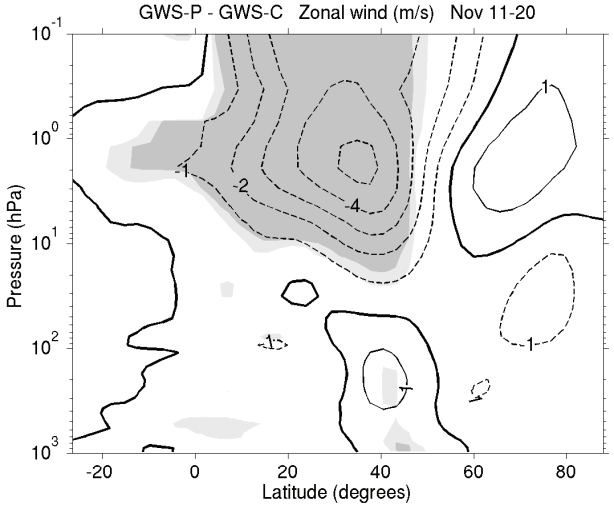
GWS-P - GWS-C Zonal wind (m/s) Nov 11-20
Pressure (hPa)
Latitude (degrees)

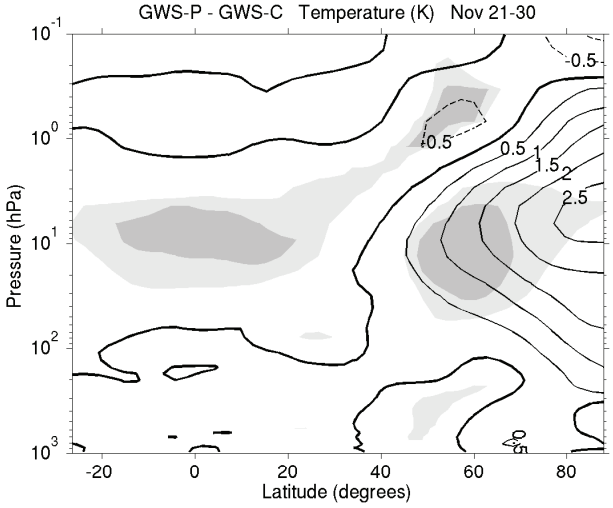
GWS-P - GWS-C Temperature (K) Nov 21-30
Pressure (hPa)
Latitude (degrees)

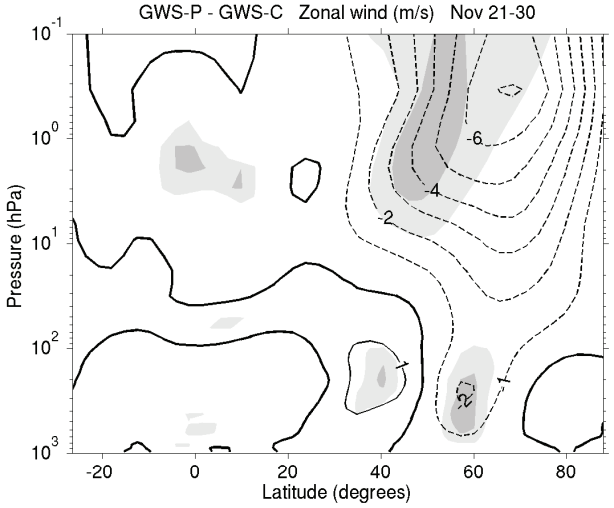
GWS-P - GWS-C Zonal wind (m/s) Nov 21-30
Pressure (hPa)
Latitude (degrees)

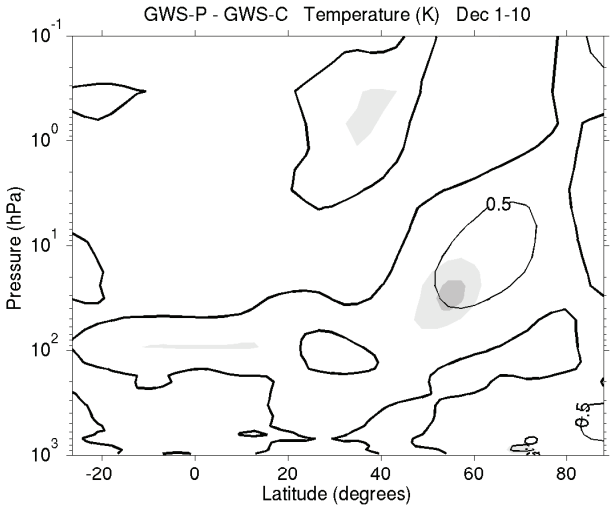
GWS-P - GWS-C Temperature (K) Dec 1-10
Pressure (hPa)
Latitude (degrees)

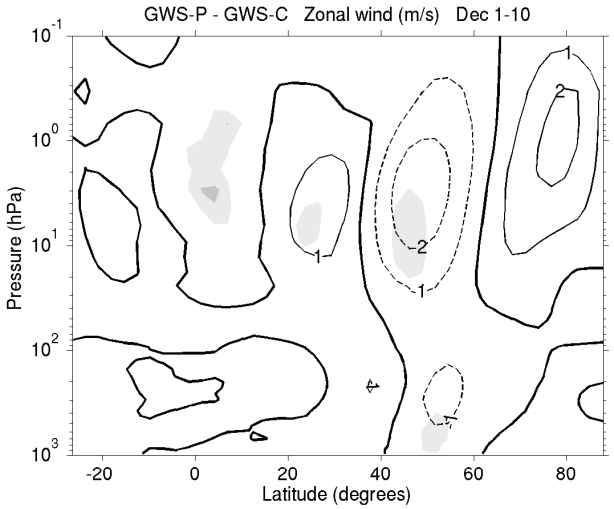
GWS-P - GWS-C Zonal wind (m/s) Dec 1-10
Pressure (hPa)
Latitude (degrees)

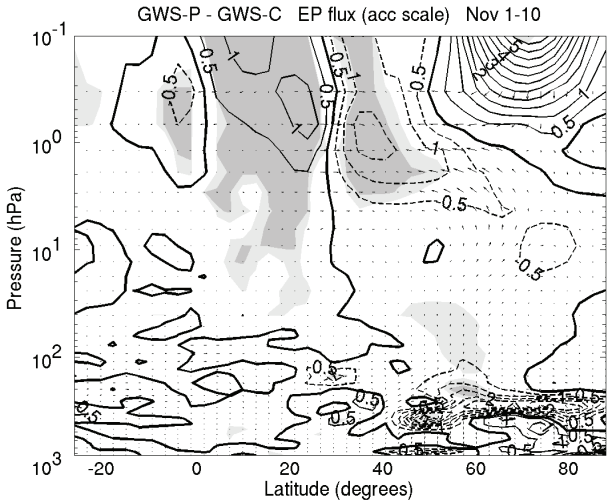
GWS-P - GWS-C EP flux (acc scale) Nov 1-10
Pressure (hPa)
Latitude (degrees)

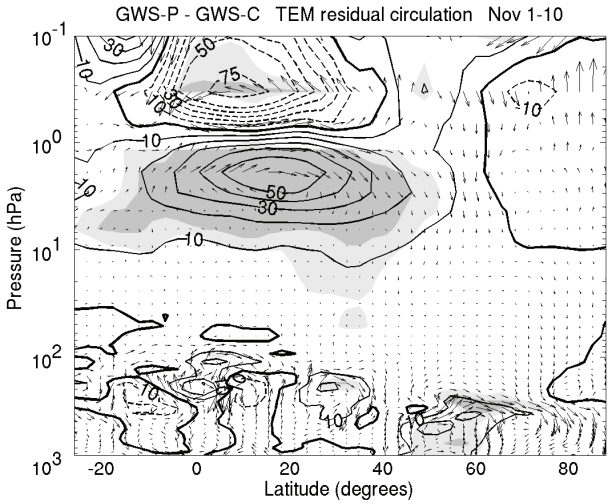
GWS-P - GWS-C TEM residual circulation Nov 1-10
Pressure (hPa)
Latitude (degrees)

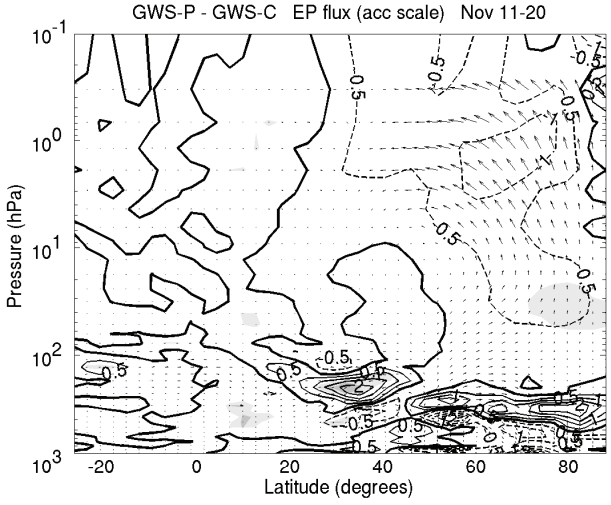
GWS-P - GWS-C EP flux (acc scale) Nov 11-20
Pressure (hPa)
Latitude (degrees)

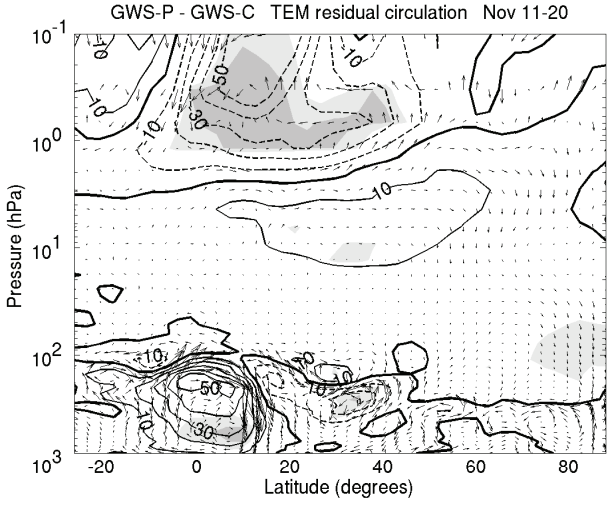
GWS-P - GWS-C TEM residual circulation Nov 11-20
Pressure (hPa)
Latitude (degrees)

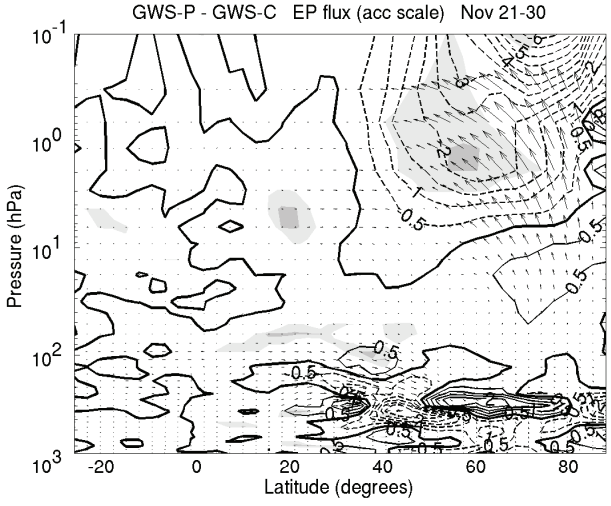
GWS-P - GWS-C EP flux (acc scale) Nov 21-30
Pressure (hPa)
Latitude (degrees)

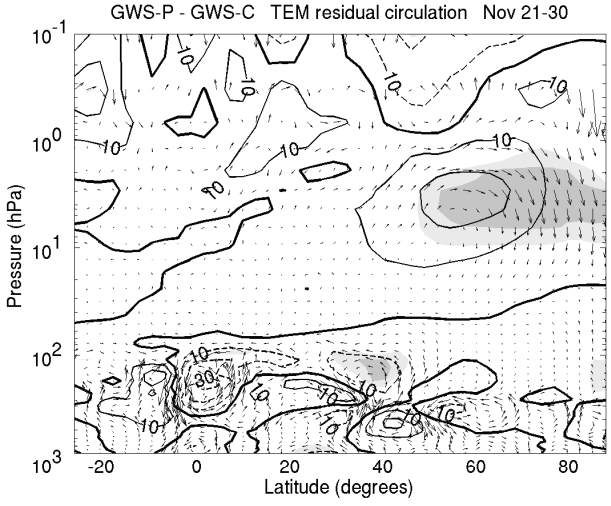
GWS-P - GWS-C TEM residual circulation Nov 21-30
Pressure (hPa)
Latitude (degrees)

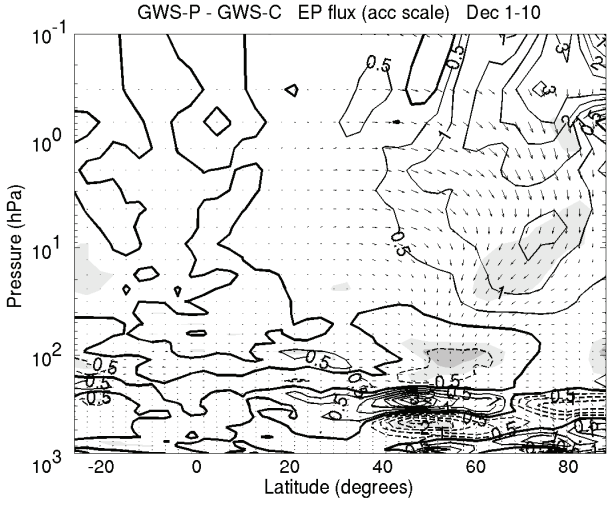
GWS-P - GWS-C EP flux (acc scale) Dec 1-10
Pressure (hPa)
Latitude (degrees)

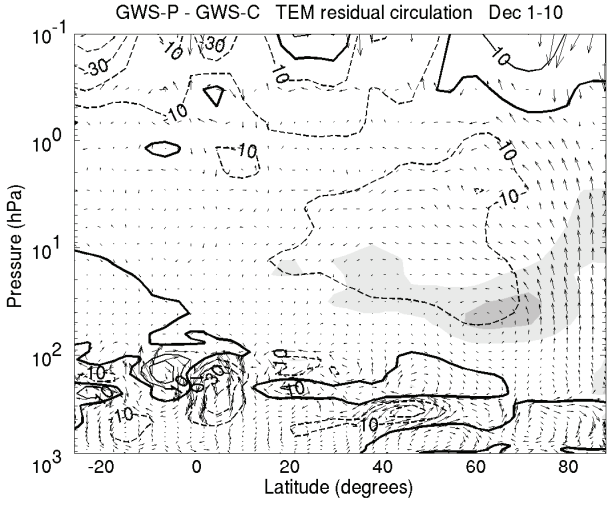
GWS-P - GWS-C TEM residual circulation Dec 1-10
Pressure (hPa)
Latitude (degrees)

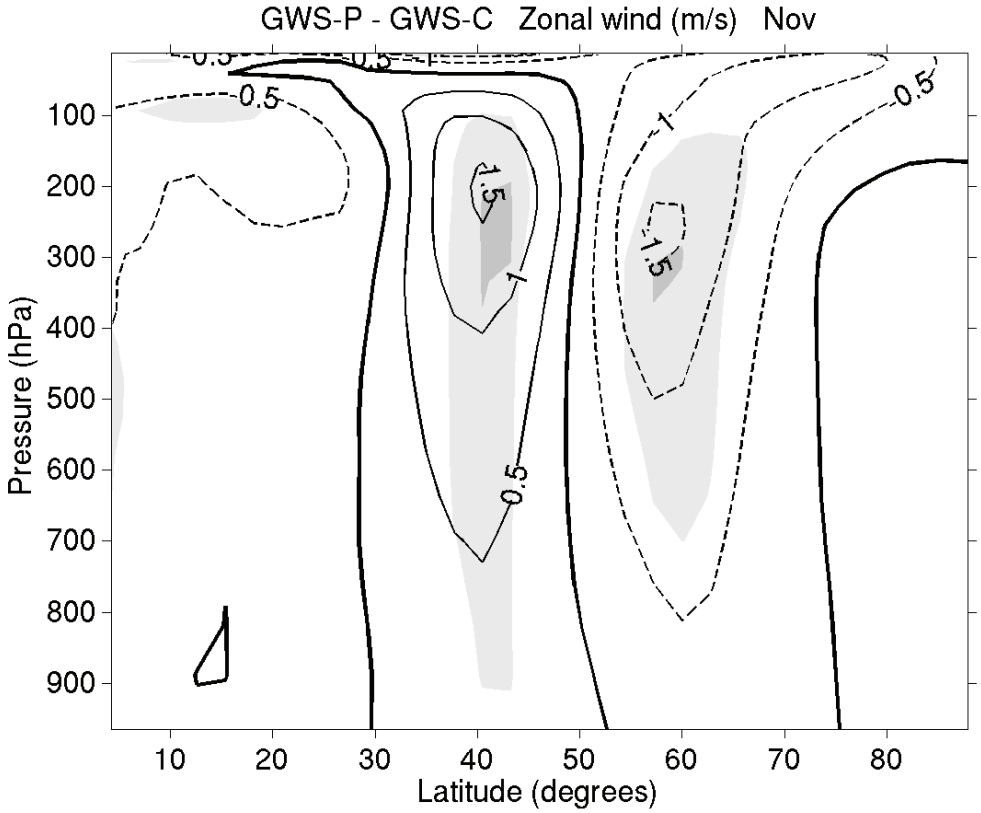
GWS-P - GWS-C Zonal wind (m/s) Nov
Pressure (hPa)
Latitude (degrees)
100
200
300
400
500
600
700
800
900
10
20
30
40
50
60
70
80
0.5
1
1.5

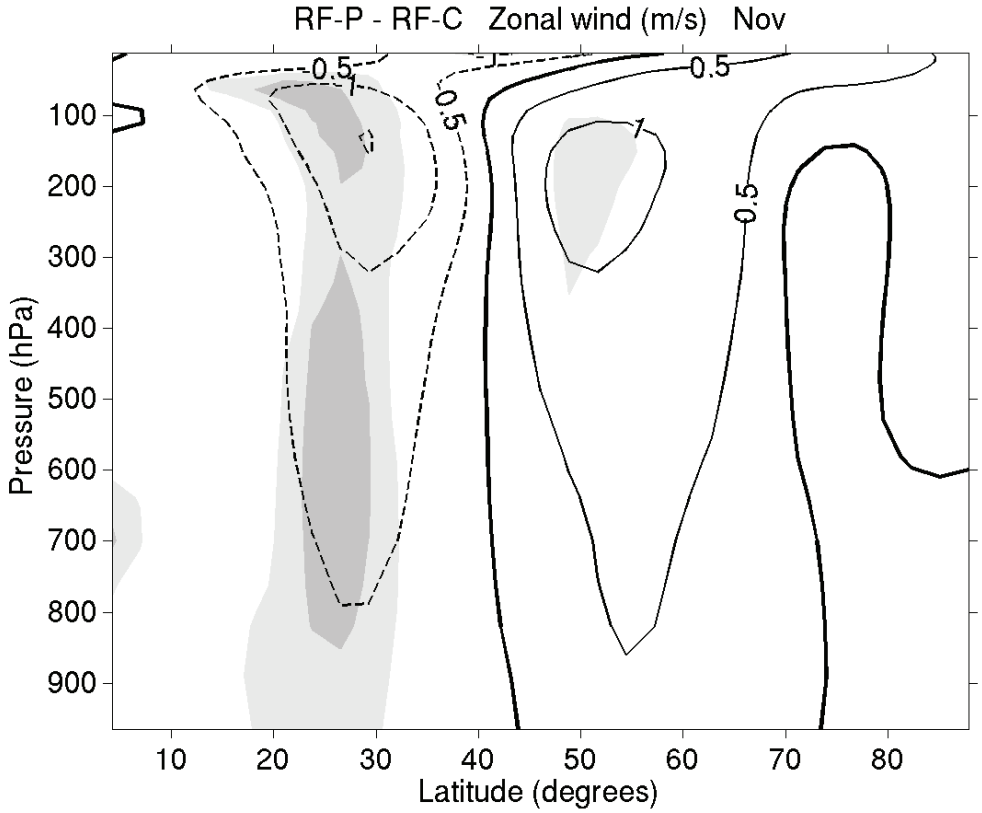
RF-P - RF-C Zonal wind (m/s) Nov
Pressure (hPa)
Latitude (degrees)
100
200
300
400
500
600
700
800
900
10
20
30
40
50
60
70
80
0.5
1

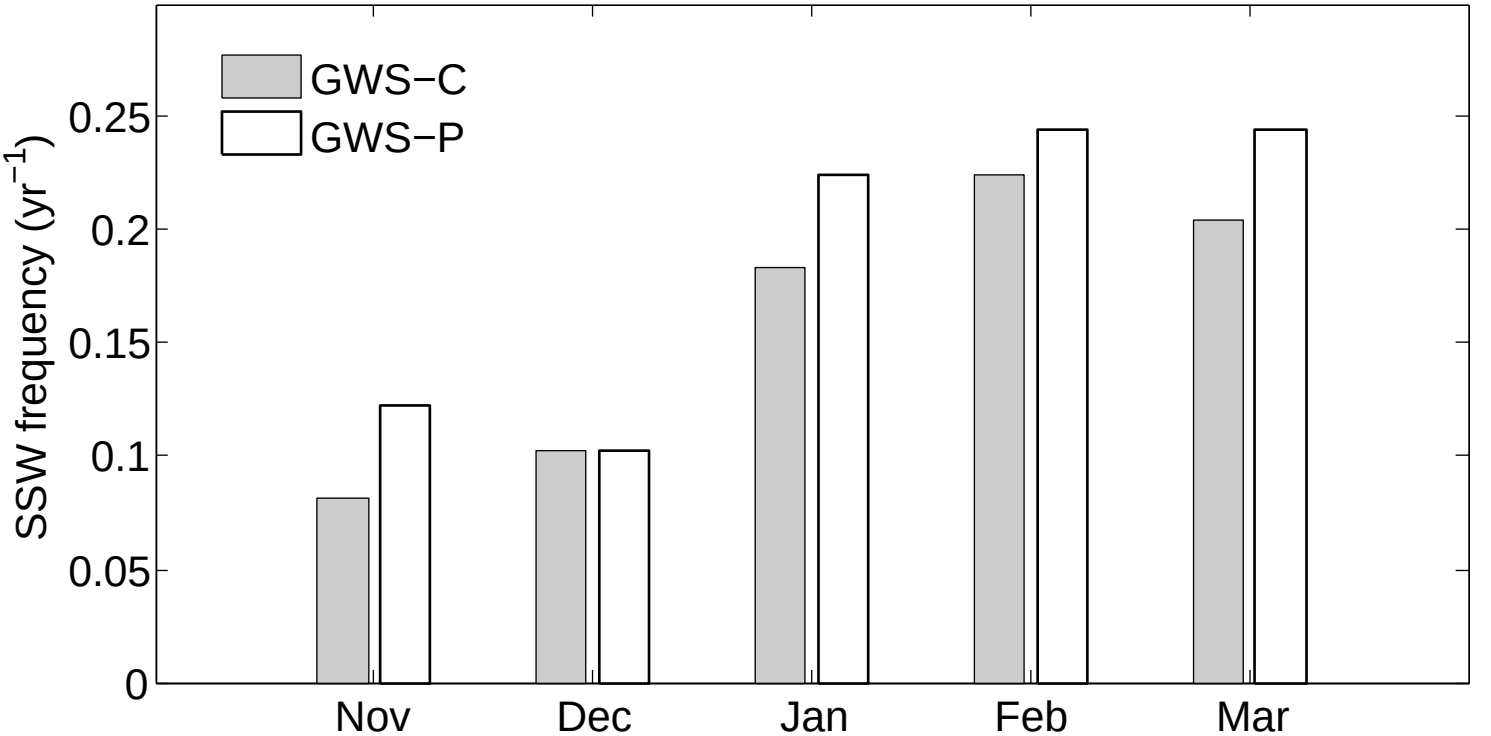
GWS−C
GWS−P
SSW frequency (yr^{-1})
0
0.05
0.1
0.15
0.2
0.25
Nov
Dec
Jan
Feb
Mar

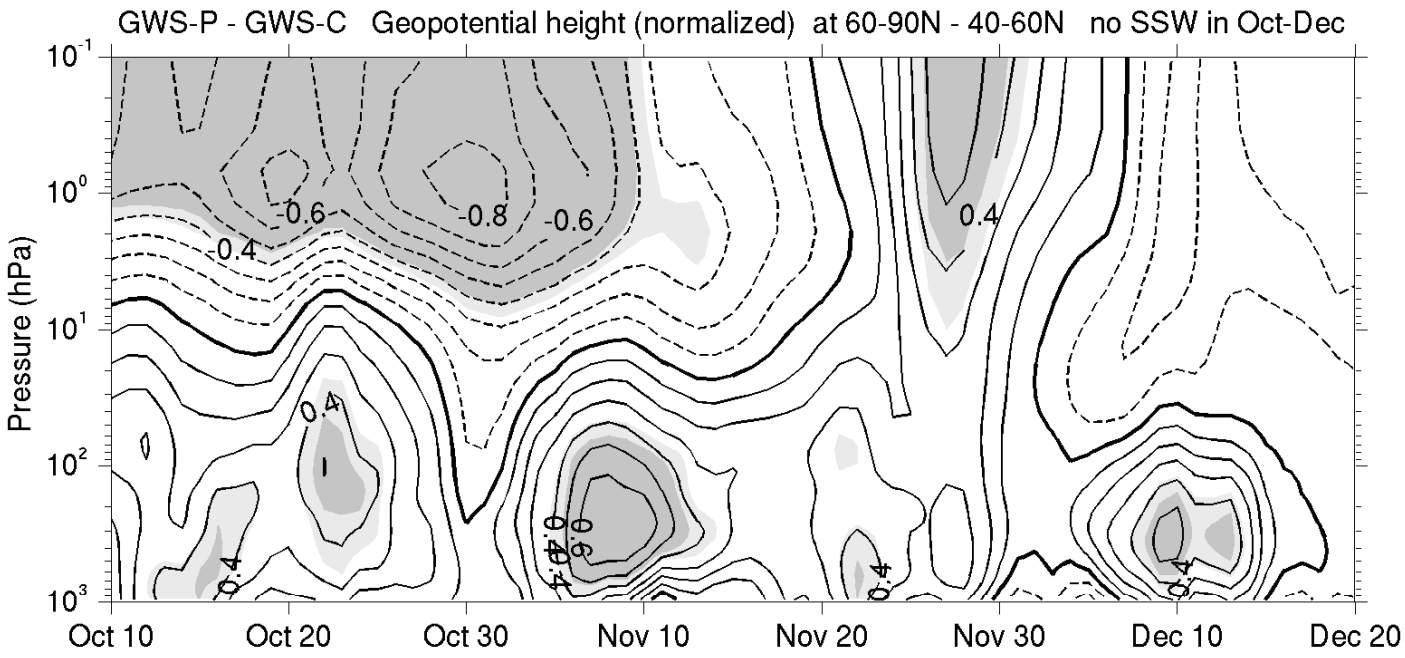
GWS-P - GWS-C Geopotential height (normalized) at 60-90N - 40-60N no SSW in Oct-Dec
Pressure (hPa)
10^-1
10^0
10^1
10^2
10^3
Oct 10
Oct 20
Oct 30
Nov 10
Nov 20
Nov 30
Dec 10
Dec 20
-0.6
-0.8
-0.6
-0.4
0.4
0.4
0.6
0.4
0.4
0.4

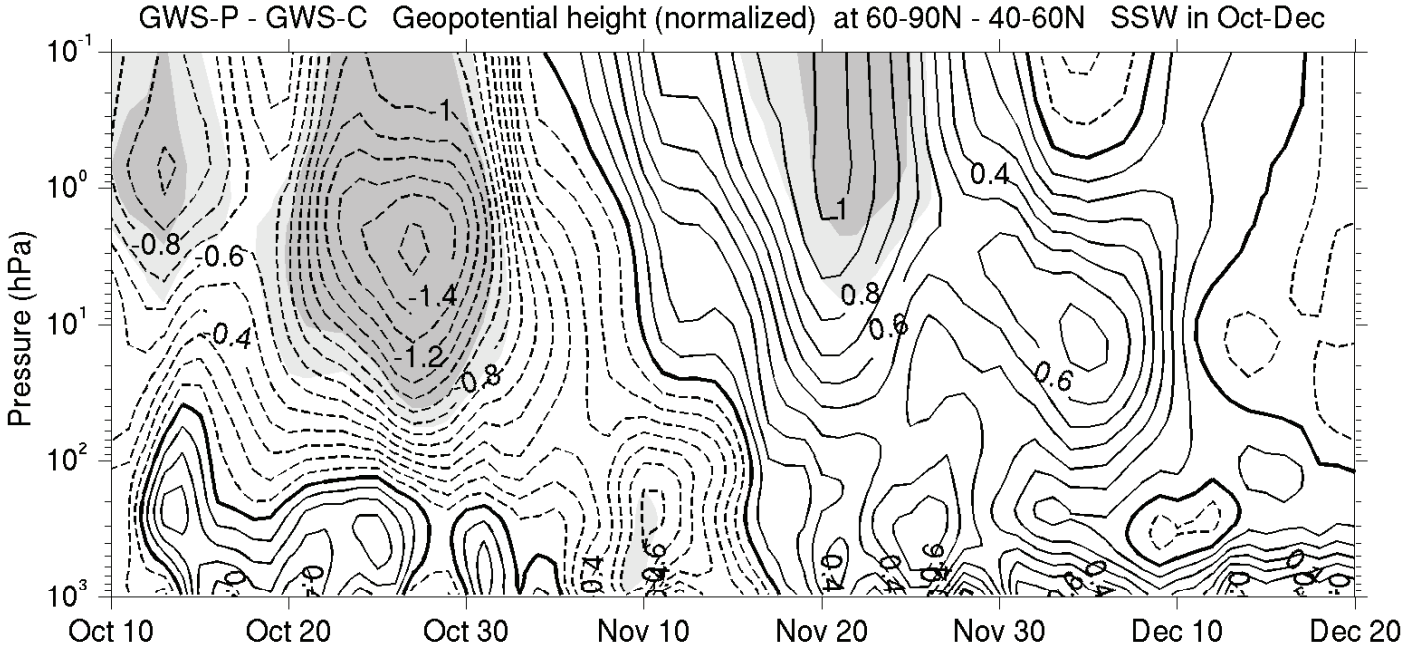
GWS-P - GWS-C Geopotential height (normalized) at 60-90N - 40-60N SSW in Oct-Dec
Pressure (hPa)
10^-1
10^0
10^1
10^2
10^3
Oct 10
Oct 20
Oct 30
Nov 10
Nov 20
Nov 30
Dec 10
Dec 20
-1
-0.8
-0.6
-1.4
-0.4
-1.2
-0.8
1
0.4
0.8
0.8
0.6